Mechanistic details of the formation and growth of nanoscale voids in Ge under extreme conditions within an ion track

Hooda, Sonu

2017-06-07

Hooda , S , Avchachov , K , Khan , S A , Djurabekova , F , Satpati , B , Nordlund , K , Bernstorff , S , Ahlawat , S , Kanjilal , D & Kabiraj , D 2017 , ' Mechanistic details of the formation and growth of nanoscale voids in Ge under extreme conditions within an ion track ' , Journal of Physics. D, Applied Physics , vol. 50 , no. 22 , 225302 . https://doi.org/10.1088/1361-6463/aa6e25

http://hdl.handle.net/10138/308772
https://doi.org/10.1088/1361-6463/aa6e25

Preprint of paper published as Journal of Physics. D, Applied Physics. 50, 22 (2017) 225302.

Mechanistic details of the formation and growth of nanoscale voids in Ge under extreme conditions within an ion track

Sonu Hooda[1], Konstantin Avchachov[2], S. A. Khan[1], Flyura Djurabekova[2], Kai Nordlund[2], B. Satpati[3], Sigrid Bernstorff[4], Sarita[5], D. Kanjilal[1], D. Kabiraj[1]

[1]*Inter-University Accelerator Centre, Aruna Asaf Ali Marg, New Delhi-110067, India*

[2] *Saha Institute of Nuclear Physics, 1/AF, Bidhannagar, Kolkata-700064, India*

[3]*Department of Physics and Helsinki Institute of Physics, University of Helsinki, 00014 Helsinki, Finland*

[4]*Sincrotrone Trieste, SS 14 km163,5, 34012 Basovizza, Italy*

[5]*Bhabha Atomic Research Centre, Mumbai 400 085, India*

Abstract

The initial steps of Ge nanovoids formation have been studied. Two step energetic ion irradiation processes was used to fabricate novel and distinct embedded nanovoids within bulk Ge. The formation of voids in amorphous-Ge (a-Ge) and their size, and shape evolution under ultra-fast thermal spike within ion track of swift heavy ion, is meticulously expatiated using experimental and theoretical approaches. The 'bow-tie' shape of void formed in single ion track tends to attain spherical shape as the ion tracks overlap at about 1×10^{12} ions cm^{-2} and the void assumes prolate spheroid shape with major axis along the ion trajectory at sufficiently high ion fluences. Small angle X-ray scattering can provide information about primary stage of void formation hence this technique is applied for monitoring simultaneously their formation and growth dynamics. The results are supported by transmission (XTEM) and scanning (XSEM) electron micrographs. The multi-time-scale theoretical approach corroborate the experimental findings and relate the bow-tie shape void formation to density variation as a result of melting and resolidification of Ge within thermal spike generated along ion track plus non-isotropic stresses generated towards the end of the thermal spike.

Introduction

Nanostructured semiconductors have attracted widespread attention from broad scientific community due to their unique quantum-confined nanoscale properties. In particular, physical properties of micro and nanoporous semiconductors have been the subject of numerous studies during the past decades. Germanium (Ge) is one of these material receiving substantial attention which has been extensively investigated and matured to industrial applications recently. Moreover, fabrication of nano-scale voids in the bulk and on the surface of a-Ge is important as porosity plays an important role in visible photoluminescence [1,2] from porous Ge which is realized as a key to the future optoelectronic device fabrication. Porous materials can have numerous surface chemistry related applications due to the porosity induced increase in surface area [3]. Furthermore, through its tailoring, porous material can be functionalized and also used as filters [4], gas sensors [5], thermoelectric elements [6], solar cells [1] and high efficiency anodes for electric batteries [7].

Ion beam induced process is a superior technique to overcome the drawbacks of conventional methods of porous structures formation [2,8,9] as the latter incorporates chemical contamination in the sample along with the porous structures. Moreover, in conventional techniques, there is no uniformity of porosity and directionality e.g. <113> is a preferred direction in Si [10,11] that is quite unexplained still. As compared to the conventional porous structure fabrication method like anodization or chemical etching [8], ion beams may be used to synthesize pores with controlled size and positions without contamination. Production of these voids can be controlled by varying the ion beam parameters such as energy, fluence, angle of irradiation etc. [12,13]. This enables porous layer formation in pre-amorphized region with predefined three dimensional void structures. Furthermore, swift heavy ion (SHI) induced void formation is independent of their electrical properties and restricted to a-Ge only as c-Ge is rather insensitive to electronic energy loss (S_e) [3,14]. The fascinating applications underscore the basic interest in theoretical understanding of formation of voids in Ge using ion beam irradiation. Well-defined nanostructures were reported within amorphous Ge during bombardment with energetic heavy ions eventually resulting in nanohole patterns [15], nanoporous or sponge-like structures[16]. Moreover, nanoholes, nanodot pattern and porous structure formation at the surface has been reported in Ge under keV ion irradiation in recent years [17,18]. Despite the increasing interest in void formation in Ge, nanostructure formation on Ge surface due to high energy ion irradiation has been studied to a much lesser extent along with less understanding. Recently, the S_e effect of SHI on void formation in a-Ge layers is

reported by few groups. Gartner *et al.* [19] reported that outgoing shock waves, resulting from transient heating and expansion of the ion-track core due to SHI irradiation, is the origin of voids. Our group also studied response of pre-damaged Ge under 100 MeV Ag ions irradiation [20,21] to report the growth dynamics and shape evolution of voids [3]. For the sake of completeness, surface modification due to high energy ion irradiation in Ge and role of electronic sputtering on these surface pattern formations was also presented [14,22]. Ridgway *et al.* [13] reported the SHI induced bow-tie shape void formation resulting from the melting of Ge during thermal spike and its re-solidification. Due to detection difficulties of amorphous ion tracks in an amorphous matrix using transmission electron microscopy (TEM), the small angle x-ray scattering (SAXS) technique was employed by Ridgway *et al.* [13] for characterizing ion tracks and voids formed in single track. Moreover, glancing incidence small-angle x-ray scattering (GISAXS) is an effective means to quantify the growth dynamics of voids in terms of dimensions in both in-plane and out-of-plane orientations. GISAXS technique is well established and widely used to study formation and modification of nanostructures especially by ion beams [23-25]. This technique is suitable to study nano porous structures as X-ray scattering is highly sensitive to contrast of electron density in medium [26].

In present report, we utilized GISAXS and microscopy techniques (like TEM, SEM) to study the formation and growth dynamics of voids in a-Ge. A multi-time-scale theoretical approach including an asymptotical trajectory Monte Carlo (MC) calculation of the electron dynamics, a two-temperature model (TTM) description of the heat dissipation and a MD simulation of the atom dynamics for ion tracks in a-Ge is also used for corroborating the experimental findings. Using this novel approach, we have investigated the shape evolution of void in ion-track experimentally and substantiated theoretically.

Experimental Details

Pre-amorphization of c-Ge wafer was carried out using Ar ion implantation of four energies varying from 0.3 to 2 MeV resulting in an amorphous Ge layer of thicknesses ~1.2 μm on c-Ge. The damage introduced by irradiation was estimated to be 7 DPA (displacement per atom) as calculated using Monte-Carlo simulation SRIM [27]. Subsequent irradiation was performed of these samples with 100 MeV Ag ions (nuclear stopping power S_n= 0.1 keV nm^{-1}, S_e= 16.4 keV nm^{-1}) [27] to ion fluences ranging between 1×10^{11} and 1×10^{13} ions cm^{-2}. The beam was delivered from Pelletron accelerator at IUAC (Delhi), with controlled ion flux of ~ 1×10^{10} ions cm^{-2} s^{-1}. Here S_n/S_e being ~10^{-3}, energy loss by electronic process dominates over nuclear

energy loss and ensuring uniform energy deposition within damaged layer due to significantly higher range of Ag ion (~12 μm) as compared to the extent of the amorphous layers. Multiple techniques such as synchrotron based Glancing Incidence Small Angle X-Ray Scattering (GISAXS), Field Emission Scanning Electron Microscopy (FE-SEM) [MIRA-II LMH, TESCAN] in cross-section mode, Cross section transmission electron microscopy (XTEM) and Molecular Dynamics (MD) simulations have been applied to derive models that describe the formation and growth dynamics of open volume in a-Ge under energetic ion irradiation. Electron beam of energy 7 keV and 300 keV was used to capture the SEM and XTEM images, respectively. XTEM was performed in the present case using FEI, Tecnai, F30-ST. GISAXS measurements were performed at the SAXS beamline in synchrotron ELETTRA, Trieste (Italy) [28] using the X-ray beam energy 8 keV ($\lambda = 0.154$ nm). The use of grazing angle, α_i, with respect to the sample surface minimizes the undesirable scattering from the bulk and enhances the near-surface scattering. Hence, GISAXS spectra were recorded at an angle of incidence of 1° to maximize the contribution from the voids containing layer and to avoid contribution from the crystalline Ge beneath it. The scattering intensity spectra of x-rays were acquired by a two-dimensional position sensitive detector PILATUS 1M, placed perpendicular to the incident beam, at a detector to sample distance of $L \approx 2000$ mm. These GISAXS spectra were recorded by keeping the experimental condition constant, like duration of measurement, glancing angle of x-ray and detector distance to avoid any uncertainty on comparing within the samples. A schematic diagram presenting the experimental setup is shown in figure 1. The wave vectors corresponding to incident (k_i) and reflected (k_f) beam form angles α_i and α_f with the sample surface, respectively. On the other hand, the angle subtended by the scattered wave with the x-axis is denoted by $2\theta_f$. Scattered intensity I (q_y, q_z) recorded by the detector corresponds to a collective momentum transfer by an assembly of particles. The horizontal direction in the detector probes the reciprocal space along coordinate parallel to the surface. Therefore, q_y gives information about the correlations parallel to the surface like cluster correlation distance and cluster radii. The vertical direction in the detector probes the reciprocal space coordinate perpendicular to the surface. DPDAK software has been utilized to extract and integrate the line profiles (along y and z direction) from raw data [29]. The size distribution of voids was quantified by analysing the projected data using structure factor of different shapes for a best fit.

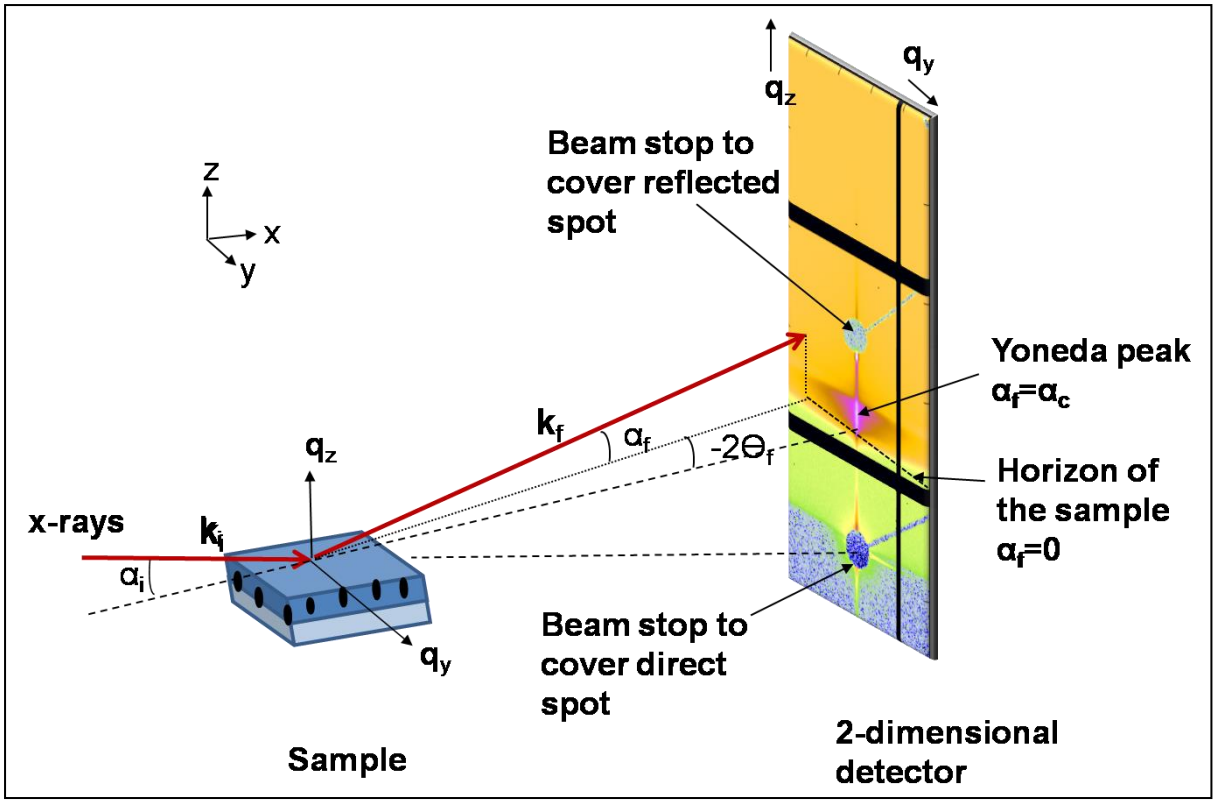

Figure 1: Geometry of GISAXS setup; α_i and α_f are the incident and exit angles respectively with respect to sample surface. $2\Theta_f$ is the in-plane angle made by scattered beam.

Experimental Results

1. Glancing Incidence X-Ray Scattering (GISAXS)

GISAXS is considered to be powerful technique to study microscopic inhomogeneities in samples. It can supply statistically averaged information about the morphology, structure, size distributions, number density etc. of the microstructure changes. In present case, GISAXS has been utilized to probe the voids in the ion irradiated a-Ge over wide q-range. Figure 2 (a-d) show the 2D GISAXS spectra of porous Ge consisting of scattered X-ray intensity distribution for 1° angle of incidence, as a function of ion dose. Following reference [29], discrete sections of the images were analysed separately to extract structural information contributing to the scattering in Pilatus detector. The coordinates of the scattering vector components are q_y and q_z along horizontal and vertical directions respectively where x-axis is considered as direction of incident x-ray beam.

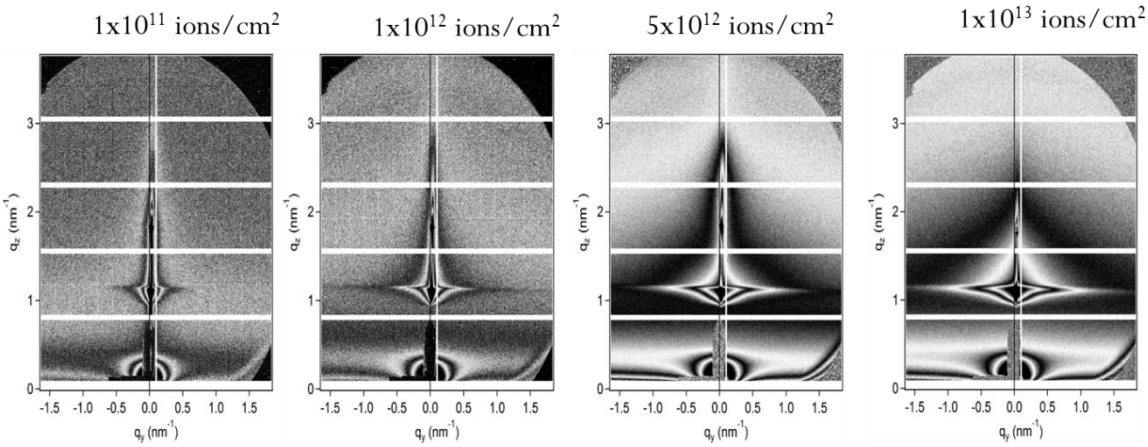

Figure 2. The 2D-GISAXS images of the a-Ge irradiated with Ag ions for different ion fluences

The horizontal and vertical projections in 2-D raw data extract the line profile of scattering intensity versus scattering vector q and the coordinates of the scattering vector at direct beam position were marked as origin. The most prominent feature in the q_z direction is the intensity maxima where the exit angle equals the critical angle (α_c) called Yoneda peak [30]. The critical angle for Ge is about 0.31° (for 8 keV x-rays) and it is directly linked to the electron density of the target medium [31] which in turn is a measure of porosity of the sample. The amplitude of scattered X-ray is given by the Fourier transformation of electron density as given by the following equation [33]:

$$A(q) = k\int_{-\infty}^{+\infty} \rho(r)\exp(-iq.r)dr \qquad .....(1)$$

Where r is the distance of point scatterer (electrons) from origin, $\rho(r)$ is the density function and q is scattering vector. The line profiles along q_y direction for a fixed q_z value about the Yoneda region for all samples are shown in figure 3 (a) [32]. The line profile along q_z direction for a fixed q_y width (centred at left side of the direct spot of X-ray i.e. q_y=0) is plotted in figure 3 (b). The variation of intensity against scattering vector is shown on a log-log plot. The scattering intensity increases in high-q region with increasing ion fluence, signifying that the contribution from the smaller particles or voids becomes higher. Scattering intensity, $I(q_y,q_z)$, is proportional to $S(q_y,q_z)[F(q_y,q_z)]^2$, where $S(q_y,q_z)$ is the total interference function and $F(q_y,q_z)$ is the particle form factor or intra-particle factor which represents the scattering from one particle. Total interference function is the Fourier transform of the particle auto-correlation function which describes the spatial arrangement of particles on the surface where correlation function corresponds to the probability of finding a scatterer at a particular position. Particle form factor is the Fourier transform of the electron density correlation function. The

different particles scatter X-rays independently and their sum gives the total scattering intensity. Since the voids are randomly distributed and there may be a size distribution as well, we use assumption of poly-dispersed particles. The GISAXS data were analysed using the software SASFIT [34]. To analyse the contribution from open volume with different shapes in the resultant scattered intensity, the form factor *F (q)* for different shapes like plate, cylinder and sphere were used for best fit of the data. The solid lines are fits to the spectra using the software as described above. Since the scattering measurements are performed in reciprocal space, the larger size inhomogeneities are contributing to scattered intensity at lower q region and vice versa. The described method revealed the average shape and size of voids as given in the table below.

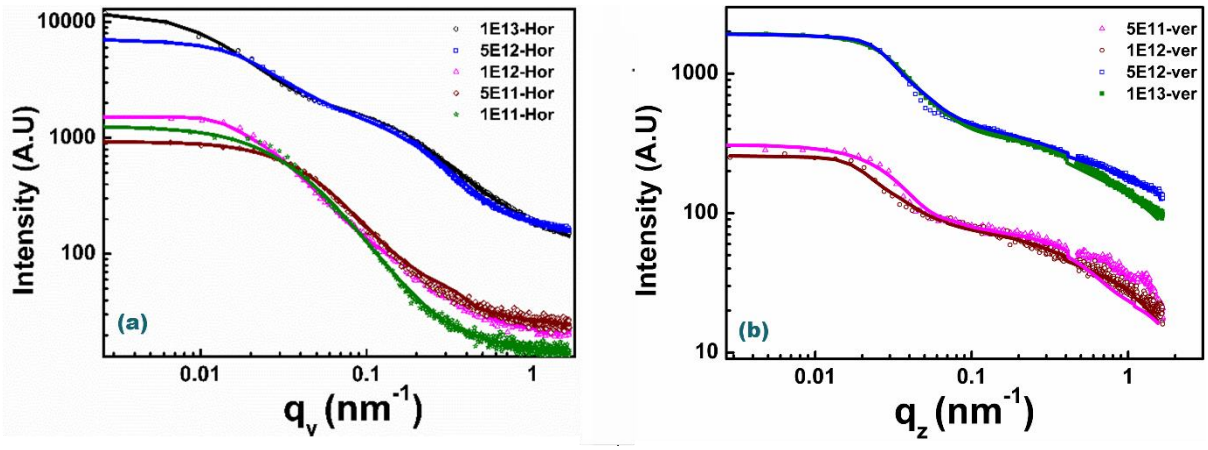

Figure 3. Fitted line profile from the GISAXS data along (a) q_y for same q_z width and; (b) q_z for same q_y

Table. Size and shape of voids extracted from GISAXS data after fitting

Ion fluence (ions cm^{-2})	**Dimension of the voids (nm)**		**Shape of voids**
	Out-of-plane	**In-plane**	
1×10^{11}	10.2	4.2	Plate
5×10^{11}	11	4.5	Plate
1×10^{12}	16.8	16.8	Sphere
5×10^{12}	22	22	Sphere
1×10^{13}	26	26	Sphere

As can be seen from Table 1, the ion irradiation creates plates like voids which are actually bow-tie shaped as described in the next section. The ion passing nearby these voids, as the fluence increases, increased their volume and change the shape. At about 1×10^{12} ions/cm^2, the voids assume spherical shape as the ion tracks are expected to overlap. With further increase in fluence, their diameter is found to increase from this analysis.

2. Microscopy results

The XTEM image shown in figure 4(a) presents the formation of voids in a-Ge recorded after irradiation to 5×10^{11} Ag ions cm^{-2} which is most probably due to single ion impact. The image shows that the shape of the void resembles that of 'bow-tie' which was also reported by Ridgway *et al.* [13]. With the help of MD simulations, they could reproduce the bow-tie shape of void. They have considered the formation of such voids within ion track during rapid re-solidification due to the higher density of liquid Ge as compared to solid Ge. From the image of the void shown in figure 4(a), its dimension can be estimated to be ~4 nm along and ~8 nm perpendicular to the ion beam. However, the shape of void is transformed from bow-tie to nearly spherical at higher ion fluence as can be seen from figure 4(b) which presents an XSEM image acquired from the sample irradiated to 5×10^{12} Ag ions cm^{-2}.

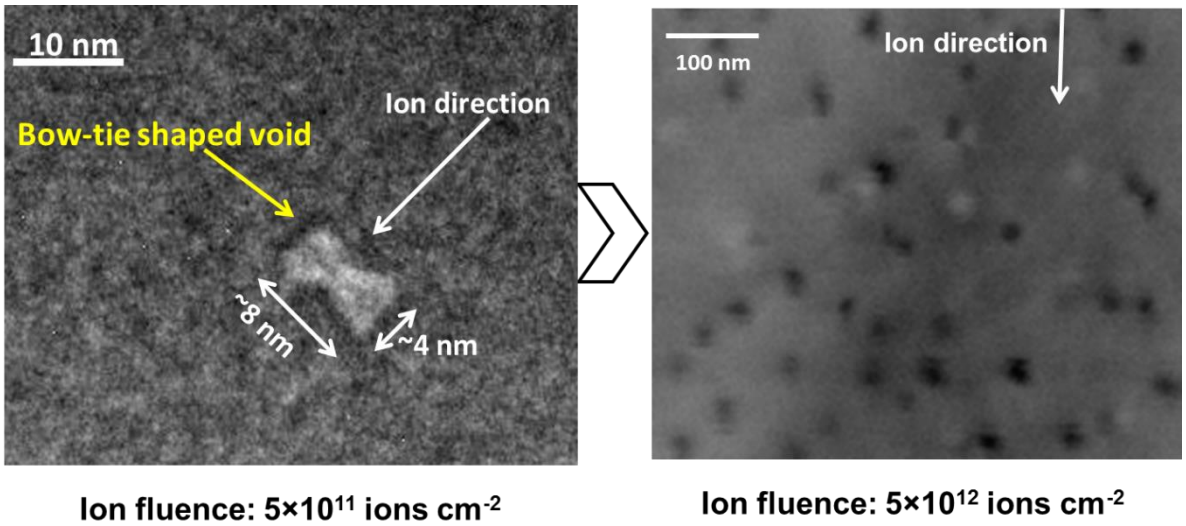

Figure 4. (a) Cross-sectional TEM image of sample irradiated to 5×10^{11} Ag cm^{-2} i.e. showing that sample is consisting of bow-tie voids due to single ion impacts (b) XSEM image of sample irradiated to 5×10^{12} Ag cm^{-2} showing the spherical voids of diameter ~20 nm after overlapping ion impacts.

Discussion

The c-Ge was observed to be insensitive to ionizing part of deposited energy from 100 MeV Ag ions. However, the irradiation of a-Ge with same ion leads to remarkable structural modifications. The void formation in a-Ge, after Ag ions irradiation can be understood on the basis of inelastic thermal spike model (I-TS) which describes SHI interactions with matter [35]. The target can be divided in two subsystems (i) the electronic and (ii) the lattice subsystem. The energy of incident Ag ion is shared between the target electrons. This energy stored in the electronic system is transferred to the atomic system via electron–phonon (e-p) coupling which finally leads to a transient rise in temperature locally. The electrons are confined within a cylindrical track along ion path and their confinement has strong influence on e-p coupling strength (g). Here, I-TS is used to describe the rise in temperature of lattice. The detailed description of two temperature model is given in our previous reports[20-22], where the temperature rise, formation of track and diameter of track were calculated in c-Ge and a-Ge. In case of c-Ge, the value of 'g' is low enough such that 100 MeV Ag produce no lattice defects that corroborate the results showing insensitivity of c-Ge towards S_e. Whereas in a-Ge, it leads to molten track formation with diameter~10 nm. Consequently, melting and re-solidification with efficient e-p coupling results in void formation due to higher density of Ge in liquid phase as compared to solid phase [13] which is inferred from the molecular dynamics simulation discussed in following sub-section.

Molecular Dynamics Simulations

Molecular dynamics (MD) simulations, using PARCAS code[36], were performed to get insight of void formation within ion track and modification of existing voids by multiple overlap of these tracks. The results from simulations demonstrating formation of bow-tie shaped voids in a-Ge due to single ion impact have been reported earlier[13]. The simulations have been extended here to study the effect of subsequent ion track on the shape and size of these bow-tie shaped voids. The volume of the simulation cell was 61×41×41 nm^3 having about 4.5 million germanium atoms which were initially arranged on c-Ge lattice. This c-Ge simulation cell was transformed into a-Ge by the approach introduced by Wooten et al.[37].

As discussed earlier, the impact of SHI can locally and transiently melt the a-Ge around its trajectory. Since Ge has higher density in liquid state as compared to solid state, this means that SHI can produce transient density changes from low to high during melting and vice versa on re-solidification. Therefore, the MD simulations should ideally use potentials which can accurately describe the solid to liquid and liquid to solid phase transformations in Ge. Since no

single potential served the purpose as described in Supplemental Material of reference [13], Posselt Stillinger-Weber potential [38] was used for simulations during the first 100 ps after the ion passage and Tersoff potential [39] for later time. The simulation cell had 0.6 nm wide border region in x and y directions, temperature controlled at 300 K by Berendsen thermostat[40], to cool down the heat spike generated sound/heat wave at the boundaries and thereby suppressing their reflection back to the centre of the cell.

The simulation of effect of SHI interaction with matter has to take care of several different processes like excitation of electrons accounting for the electronic stopping power and atomic displacements due to nuclear stopping power. Since nuclear stopping power is several orders smaller in comparison of electronic stopping power of 100 MeV Ag ions in Ge, the simulations account for excitation of electrons. The columbic interaction between nuclear charge of projectile with bound and free electrons in medium produce energetic electrons named as δ-electrons. These electrons have energies up to tens of eV and they scatter with lattice atoms as they travel in the material, thereby exciting additional electrons into the conduction band (impact ionization). Consequently, these energetic electrons thermalize by multiple scattering to reduce their energy to ~ 5 eV and emit phonons by electron-phonon coupling. In this work, the dynamics of excited electrons was handled using a combination of asymptotical trajectory Monte Carlo (MC) approach and two-temperature model (TTM). The MC method was used to model the dynamics of the excited electrons, having kinetic energy ≥ 5eV, which travel through the a-Ge and take part in impact ionization and electron-hole pair recombination through Auger processes. TTM, on the other hand, was used to treat the electrons, with kinetic energy 5 eV, which take part in electron-phonon coupling process. The details of TTM and the values of the related parameters can be found in the Supplement Material of reference [13]. It may be noted here that the high energy electrons treated by MC method lose their energy and start participating in electron-phonon coupling process. Therefore, the two processes MC and TTM methods cannot be performed sequentially but rather a synchronized MC-TTM approach is applied. The MC-TTM approach was applied up to 30 ps after the ion passage to extract the electron-phonon energy exchange rates which were then used as inputs to the MD simulations. The MD simulations are performed till 300 ps after an ion impact. The snapshot from the simulations is shown in Figure 5. The red broken curve shows the cross-sectional view of the void created by the first impacting ion which resembles a bow-tie in agreement with the experimentally observed shape of a void shown in Figure 4(a). In the same volume, the effect of second ion was simulated and followed for 300 ps again. The black broken curve outlines the resulting shape of the void due to the second impact. As can

be seen from Figure 5, the second impact increased the size of the existing void more prominently in the axial direction.

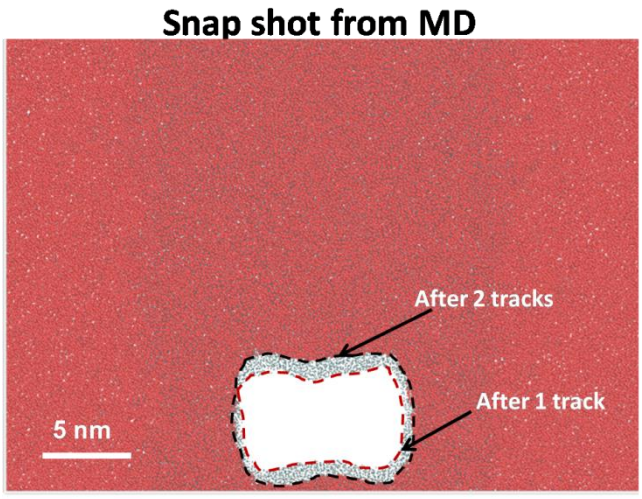

Figure 5. Superimposed snapshots from MD simulations of two consecutive 100 MeV Ag ion impacts in the centre of the simulation cell. The projection of ion trajectory is along top to bottom of the image. The volume in white is created by the first incident ion. The atoms depicted by grey circles were displaced during the heat spike generated by the second incident ion.

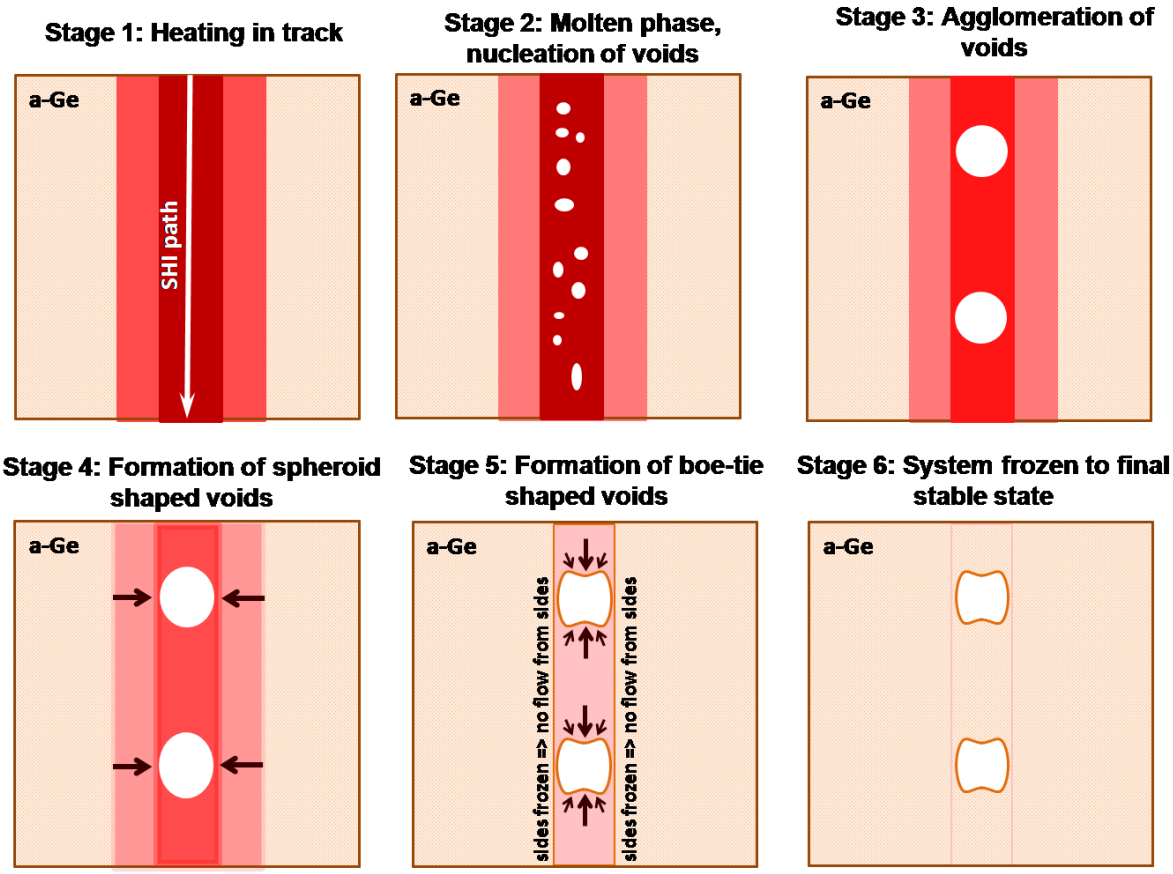

Figure 6. The schematic of various stages included in formation of void in the ion track

With the help of schematic diagram as shown in figure 6, we tried to explain bow-tie shaped void formation as proposed by Ridgway *et al.* [13]. In stage 1, as the ion passes through the material and a high temperature zone is created with Gaussian temperature distribution radially around the ion path. The thermal spike produces a radially outward material flow from the ion-track core and a phase transformation from low density solid to high density liquid in the core. In stage 2, a cylindrical molten zone is formed where voids nucleate due to higher density of Ge in liquid phase (l-Ge) as compared to Ge in solid phase. In stage 3, the small voids agglomerate to form bigger voids. When the track starts to cool, the cooling occurs from outside to inside radially in the track. In stage 4, the resolidified Ge with higher volume exerts radially inwards force which changes the shape of the voids to prolate spheroids. Arrows in the schematic indicates the direction of force. In stage 5, the expansion surrounding the still molten central volume pushes the molten material in the axial direction of the void which changes its shape to bow-tie. Finally the system freezes in this state and we observe the bow-tie shaped voids due to single ion impact, as shown in figures 5 and 4(a), with the help of MD and TEM image.

Due to multiple ion impact or overlapping of ion tracks the size of bow-tie shaped void increases as shown with the help of MD results in figure 5(a). However, the increase in size is prominent along the axial direction of ion path as compared to the radial direction. This is clear from the snapshot of MD after overlapping ion track. This axial increase in void size continues with subsequent ion track overlaps as the fluence is increased which results in a transition from bow tie- to sphere as a function of ion fluence. Moreover, it results in formation of bigger voids assuming shape of prolate spheroid on further increasing the ion fluences as discussed in our previous reports [3,14]. The shape and size evolution is estimated with the help of GISAXS results and further corroborated with the help of microscopy (XTEM and XSEM) results at higher ion fluences.

Conclusion

Swift heavy ions can induce porosity in damaged Ge as a result of void formation. The shape of the voids changes and their volume increases as the ion fluence is increased. The generation of voids in damaged Ge and their structural transformation is studied here using experimental and theoretical approaches. Experimental results, derived from XTEM, XSEM and GISAXS

investigations, showed that the shape of voids is bow-tie like at initial fluences which tends towards spherical shape as the ion tracks overlap at about 1×10^{12} ions cm^{-2}. With further increase in fluence, the voids take prolate spheroid shape with major axis along the ion trajectory. The multi-time-scale theoretical approach comprising of an asymptotical trajectory MC calculation of the electron dynamics, a TTM description of the heat dissipation and a MD simulation shed insight into the process of void formation and subsequent shape transformation. The theoretical results corroborate the experimental findings and relate the bow-tie shape to density fluctuation around ion trajectory as a result of thermal spike created in the material and non-isotropic stresses generated towards the end of the thermal spike.

Acknowledgements

[1] D. Sun, A. E. Riley, A. J. Cadby, E. K. Richman, S. D. Korlann, and S. H. Tolbert, Nature **441**, 1126 (2006).
[2] J. Shieh, H. L. Chen, T. S. Ko, H. C. Cheng, and T. C. Chu, Advanced Materials **16**, 1121 (2004).
[3] S. Hooda, S. A. Khan, B. Satpati, A. Uedono, S. Sellaiyan, K. Asokan, D. Kanjilal, and D. Kabiraj, Microporous and Mesoporous Materials **225**, 323 (2016).
[4] H. Föll, J. Carstensen, and S. Frey, J Nanomater **2006**, 10, 91635 (2006).
[5] G. Kaltsas and A. G. Nassiopoulou, Sensors and Actuators A: Physical **76**, 133 (1999).
[6] H. Goldsmid, Materials **2**, 903 (2009).
[7] N. G. Rudawski, B. L. Darby, B. R. Yates, K. S. Jones, R. G. Elliman, and A. A. Volinsky, Appl. Phys. Lett. **100** (2012).
[8] E. G. Rojas, H. Plagwitz, B. Terheiden, J. Hensen, C. Baur, G. La Roche, G. Strobl, and R. Brendel, Journal of the Electrochemical Society **156**, D310 (2009).
[9] T. S. Ko, J. Shieh, M. C. Yang, T. C. Lu, H. C. Kuo, and S. C. Wang, Thin Solid Films **516**, 2934 (2008).
[10] M. Christophersen, S. Langa, J. Carstensen, I. Tiginyanu, and H. Föll, physica status solidi (a) **197**, 197 (2003).
[11] H. Föll, M. Leisner, A. Cojocaru, and J. Carstensen, Materials **3**, 3006 (2010).
[12] T. Steinbach, J. Wernecke, P. Kluth, M. C. Ridgway, and W. Wesch, Phys. Rev. B **84**, 104108 (2011).
[13] M. C. Ridgway *et al.*, Physical Review Letters **110**, 245502 (2013).
[14] S. Hooda, S. A. Khan, B. Satpati, D. Stange, D. Buca, M. Bala, C. Pannu, D. Kanjilal, and D. Kabiraj, Appl. Phys. A **122**, 1 (2016).
[15] R. Böttger, K.-H. Heinig, L. Bischoff, B. Liedke, and S. Facsko, Appl. Phys. A **113**, 53 (2013).
[16] T. Steinbach, C. S. Schnohr, P. Kluth, R. Giulian, L. L. Araujo, D. J. Sprouster, M. C. Ridgway, and W. Wesch, Phys. Rev. B **83**, 054113 (2011).
[17] B. Roman, K. Adrian, B. Lothar, and F. Stefan, Nanotechnology **24**, 115702 (2013).
[18] S. A. Mollick, D. Ghose, and B. Satpati, Vacuum **99**, 289 (2014).
[19] K. Gärtner, J. Jöhrens, T. Steinbach, C. S. Schnohr, M. C. Ridgway, and W. Wesch, Phys. Rev. B **83**, 224106 (2011).
[20] S. Hooda, B. Satpati, T. Kumar, S. Ojha, D. Kanjilal, and D. Kabiraj, RSC Advances (2015).
[21] S. Hooda, B. Satpati, S. Ojha, T. Kumar, D. Kanjilal, and D. Kabiraj, Materials Research Express **2**, 045903 (2015).
[22] S. Hooda, S. A. Khan, B. Satpati, D. Kanjilal, and D. Kabiraj, Appl. Phys. Lett. **108**, 201603 (2016).
[23] D. Sarker, H. Kumar, R. Patra, D. Kabiraj, D. K. Avasthi, S. K. Vayalil, S. V. Roth, P. Srivastava, and S. Ghosh, J Appl Phys **115**, 174304 (2014).
[24] S. Yu *et al.*, The Journal of Physical Chemistry C **119**, 4406 (2015).
[25] S. Koyiloth Vayalil, A. Gupta, S. V. Roth, and V. Ganesan, J Appl Phys **117**, 024309 (2015).
[26] I. D. Desnica-Franković, P. Dubcek, U. V. Desnica, S. Bernstorff, M. C. Ridgway, and C. J. Glover, Nucl. Instr. Meth. Phys. Res. B **249**, 114 (2006).
[27] J. F. Ziegler, M. D. Ziegler, and J. P. Biersack, Nucl. Instr. Meth. Phys. Res. B **268**, 1818 (2010).
[28] H. Amenitsch, M. Rappolt, M. Kriechbaum, H. Mio, P. Laggner, and S. Bernstorff, Journal of synchrotron radiation **5**, 506 (1998).
[29] G. Benecke *et al.*, Journal of Applied Crystallography **47**, 1797 (2014).
[30] Y. Yoneda, Physical Review **131**, 2010 (1963).
[31] K. Devloo-Casier, K. F. Ludwig, C. Detavernier, and J. Dendooven, Journal of Vacuum Science & Technology A **32**, 010801 (2014).
[32] M. Schwartzkopf *et al.*, Nanoscale **5**, 5053 (2013).
[33] V. A. Raghunathan, Resonance **10**, 24 (2005).
[34] I. Bressler, J. Kohlbrecher, and A. F. Thunemann, J. Appl. Crystallogr. **48**, 1587 (2015).
[35] M. Toulemonde, C. Dufour, and E. Paumier, Phys. Rev. B **46**, 14362 (1992).

[36] K. Nordlund, M. Ghaly, R. S. Averback, M. Caturla, T. Diaz de la Rubia, and J. Tarus, Phys. Rev. B **57**, 7556 (1998).
[37] F. Wooten, K. Winer, and D. Weaire, Phys. Rev. Lett. **54**, 1392 (1985).
[38] M. Posselt and A. Gabriel, Physical Review B **80**, 045202 (2009).
[39] J. Tersoff, Physical Review B **39**, 5566 (1989).
[40] W. C. D. Cheong and L. C. Zhang, Nanotechnology **11**, 173 (2000).